iScience

CellPress
OPEN ACCESS

Article

Nuclear pore complex proteins are involved in centromere distribution

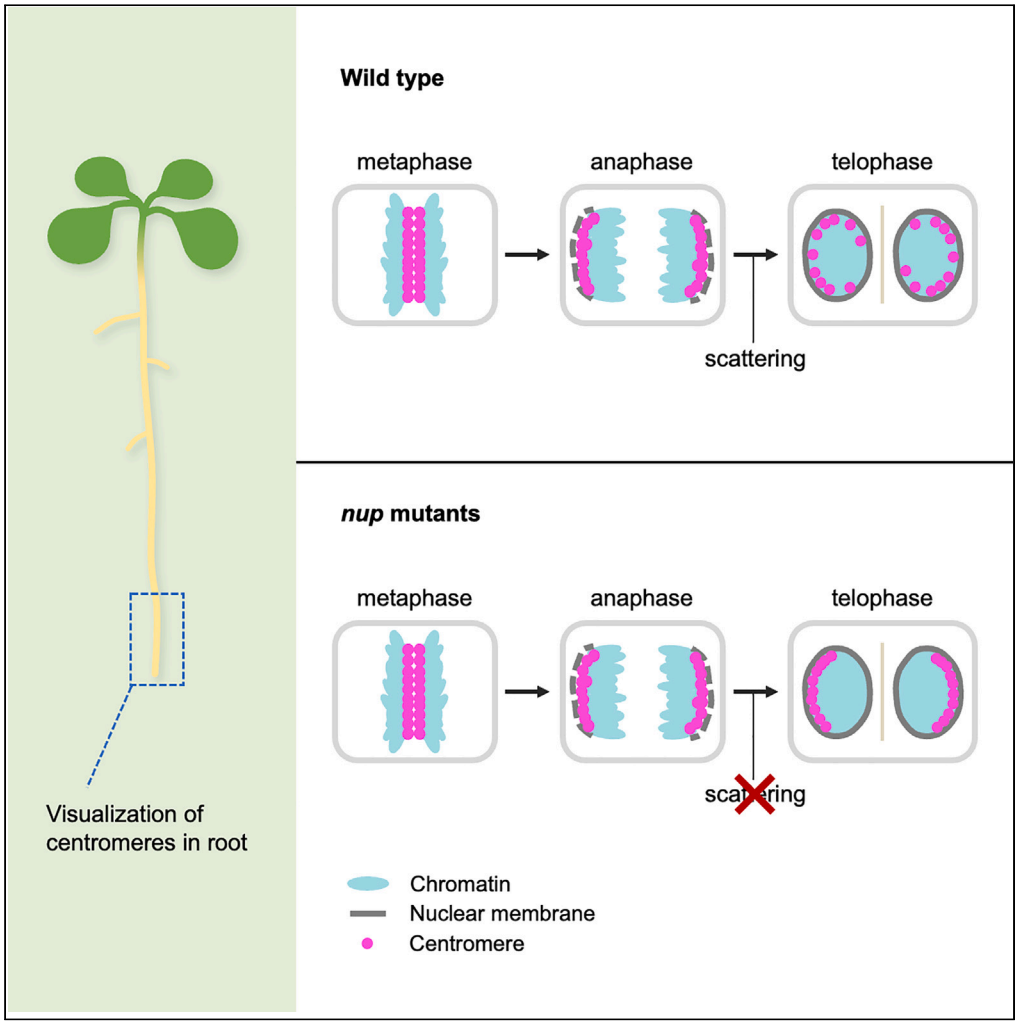

Nanami Ito, Takuya Sakamoto, Yuka Oko, Hikaru Sato, Shigeru Hanamata, Yuki Sakamoto, Sachihiro Matsunaga

sakataku@kanagawa-u.ac.jp (T.S.)
sachi@edu.k.u-tokyo.ac.jp (S.M.)

Highlights

Nucleoporins function in centromere scattering

Nucleoporins localize to centromeres in interphase and metaphase

Nucleoporins interact with the linker of nucleoskeleton and cytoskeleton complex

Nucleoporins are not involved in stabilizing the positions of centromeres

Ito et al., iScience *27*, 108855
February 16, 2024
https://doi.org/10.1016/j.isci.2024.108855

iScience

CellPress
OPEN ACCESS

Article

Nuclear pore complex proteins are involved in centromere distribution

Nanami Ito,[1] Takuya Sakamoto,[2,3,*] Yuka Oko,[3] Hikaru Sato,[1] Shigeru Hanamata,[2] Yuki Sakamoto,[4] and Sachihiro Matsunaga[1,5,*]

SUMMARY

The subnuclear distribution of centromeres is cooperatively regulated by condensin II and the linker of nucleoskeleton and cytoskeleton (LINC) complex. However, other nuclear membrane structures and nuclear proteins are probably involved in centromere dynamics and distribution. Here, we focused on the nuclear pore complex (NPC), which is known to regulate gene expression, transcription memory, and chromatin structure in addition to transport between the cytoplasm and nucleoplasm. We report here that some nucleoporins (Nups), including Nup85, Nup133, CG1, Nup93b, and NUA, are involved in centromere scattering in *Arabidopsis thaliana*. In addition, the centromere dynamics after metaphase in *nup* mutants were found to be similar to that of the condensin II mutant. Furthermore, both biochemical and genetic approaches showed that the Nups interact with the LINC complex. These results suggest that Nups regulate centromere scattering cooperatively with condensin II and the LINC complex.

INTRODUCTION

The centromere is a genomic region where kinetochores are formed during cell division.[1] There are two types of centromere positioning in eukaryotes: the Rabl and non-Rabl orientations.[2–4] In the Rabl orientation, centromeres cluster on one side of the nucleus[2]: this pattern maintains the position of centromeres in anaphase when centromeres move to the spindle pole body during chromosome segregation.[3] Meanwhile, in the non-Rabl orientation, centromeres are scattered throughout the nucleus: this pattern is formed by a dynamic change in chromosome positioning after chromosome segregation.[5,6] Which arrangement pattern is adopted varies among species. Budding yeast, fission yeast, barley, and fruit flies show the Rabl orientation,[3,7–9] while humans, mice, and *Arabidopsis thaliana* show the non-Rabl one.[10–12] Because the Rabl orientation preserves the centromere arrangement in anaphase, it is considered a primitive pattern, and it is speculated that the non-Rabl orientation was later established via the acquisition of a mechanism to scatter centromeres.[4,5,6]

In the nurse cells of *Drosophila melanogaster*, endoreplication promotes the formation of polytene chromosomes.[13] After the fifth endoreplication cycle, the chromosome positioning changes from the Rabl orientation to the non-Rabl orientation.[14] This significant change in the spatial arrangement of chromosomes is regulated by condensin II.[15] Condensin II consists of two structural maintenance of chromosome (SMC) subunits, SMC2 and SMC4, and three condensin II-specific non-SMC subunits, chromosomal associated protein (CAP)-D3, CAP-G2, and CAP-H2, and functions in mitotic chromosome condensation.[16] In the nurse cells, condensin II promotes chromosome condensation in interphase, causing clustered centromeres to scatter throughout the nucleus; thus, the Rabl orientation changes to the non-Rabl orientation.[15] In addition, in humans, condensin II regulates the formation of the non-Rabl orientation by promoting chromosome condensation in mitosis.[17] Taking these findings together, condensin II regulates the centromere positioning in animals, although the timing of its function differs among species.

We recently revealed that the centromere positioning in *A. thaliana* is determined in a two-step process, involving scattering and stabilization.[18] In the first step, condensin II plays a major role in centromere scattering from anaphase to telophase. The loss of condensin II function was shown to lead to the Rabl-like orientation.[18] In addition, the linker of nucleoskeleton and cytoskeleton (LINC) complex, which penetrates the nuclear membrane and connects the cytoplasm to the nucleoplasm, also regulates centromere scattering.[18] The LINC complex consists of the inner nuclear membrane proteins, Sad1/UNC-84 (SUN) domain proteins (SUN1-5), and the outer nuclear membrane proteins, Klarsicht/ANC-1/Syne homology (KASH) domain proteins such as SUN-interacting nuclear envelope protein (SINE)1/2, WPP domain-interacting tail-anchored protein (WIT)1/2, WPP domain-interacting protein (WIP)1/2/3.[19] Condensin II and the LINC complex form a giant complex,

[1]Department of Integrated Biosciences, Graduate School of Frontier Sciences, The University of Tokyo, Kashiwa, Chiba 277-8562, Japan
[2]Department of Science, Faculty of Science, Kanagawa University, Yokohama, Kanagawa 221-8686, Japan
[3]Faculty of Science and Technology, Department of Applied Biological Science, Tokyo University of Science, Noda, Chiba 278-8510, Japan
[4]Department of Biological Sciences, Graduate School of Science, Osaka University, Toyonaka, Osaka 560-0043, Japan
[5]Lead contact
*Correspondence: sakataku@kanagawa-u.ac.jp (T.S.), sachi@edu.k.u-tokyo.ac.jp (S.M.)
https://doi.org/10.1016/j.isci.2024.108855

CII-LINC, which cooperatively regulates centromere scattering.[18] The second step is centromere positioning, which is regulated by the nuclear lamins CROWDED NUCLEI (CRWN)1/4. CRWNs build a meshwork structure beneath the inner nuclear membrane and mechanically support the structure of the nucleus.[20] In *crwn1/4* double mutants, centromeres scattered, but their positioning was less stable: the velocity of movement was increased compared with that in the wild type.[18] Taking these findings together, we suggested a two-step model of the regulation of centromere distribution in *A. thaliana*: (i) centromeres are scattered by CII-LINC from anaphase to telophase, and (ii) the position of centromeres is stabilized by CRWNs during interphase.[18] Thus, not only condensin II but also nuclear membrane proteins have been shown to play an essential role in centromere positioning in plants.

Our previous study found that the LINC complex contributes to the scattering of centromeres, and therefore we hypothesized that other nuclear membrane proteins might also be involved in this process. Hence, we focused on the nuclear pore complex (NPC) in this study. The NPC consists of approximately 30 different nucleoporins (Nups), which comprise subcomplexes, the outer ring, the inner ring, the linker, the transmembrane ring, the channel, the nuclear basket, and the cytoplasmic filaments.[21–25] The NPC is known to function in nucleo-cytoplasmic transport,[26] but besides this canonical function, studies in yeast and animals have revealed that Nups bind to chromatin and regulate gene expression, transcription memory, chromatin structure, and DNA damage response.[27,28] In *A. thaliana*, a component of the nuclear basket subcomplex, Nup136, binds to the pericentromeric region.[29] However, little is known about Nups' function apart from in nucleo-cytoplasmic transport in plants. In this study, we tested whether the NPC is involved in centromere arrangement in *A. thaliana*. We found that the NPC components Nup85, Nup133, CANDIDATE GENE 1 (CG1), Nup93b, and NUCLEAR PORE ANCHOR (NUA) are involved in centromere scattering. Potential interaction of SUN1 with Nup85 and CG1 suggests that the NPC is involved in the first step of the two-step regulation, centromere scattering.

RESULTS

The NPC is involved in the arrangement of centromeres

To elucidate the involvement of the NPC in the arrangement of centromeres, we investigated centromere distribution in *nup* mutants. We analyzed transfer DNA insertion mutants of 12 kinds of Nups from each subcomplex of the NPC and finally prepared 16 *nup* mutant alleles for this study (Table S1). For 10 of these 16 *nup* mutants, we checked the expression levels of each *Nup* gene by quantitative RT-PCR (qRT-PCR) (Figure S1) because no reports on these levels have been published.

We visualized the distribution of centromeres in the nuclei of root tips of *nup* mutants by live imaging. We introduced *p35S::VENUS-centromeric histone H3* (*CENH3*) and *pRPS5a::H2B-tdTomato* into *nup* mutants and analyzed the degree of bias in centromere distribution using the method presented in our previous report[18] (Figure 1C). Among the 16 *nup* mutants, *nup85-1*, *nup85-2*, *nup133-1*, *cg1-2*, *cg1-3*, *nua-2*, *nua-3*, and *nup93b-1* showed significantly biased centromere distribution compared with the wild type (Figures 1A, 1C, and S2). Although *A. thaliana* has two homologs of *Nup93* (*Nup93a* and *Nup93b*), only the mutant of *Nup93b* showed abnormal centromeres distribution (Figures 1A, 1C, and S2), suggesting the functional diversity of these two homologs. The biased centromere distribution in the *nup* mutants was recovered in complementation lines (Figures 1B and 1C). These results demonstrated the involvement of Nup85, Nup133, CG1, NUA, and Nup93b in the arrangement of centromeres. Furthermore, these Nups constitute different subcomplexes of the NPC; Nup85 and Nup133 comprise the outer ring, CG1 comprises the cytoplasmic filaments, NUA comprises the nuclear basket, and Nup93b comprises the linker (Figure 1D). Therefore, it is suggested that the NPC is involved in the arrangement of centromeres.

Nups localize to centromeres in metaphase and interphase

Next, we observed the dynamics of Nups during the mitotic phase using complementation lines (Figure 1B). We chose Nup85 and NUA for observation because their expression levels were relatively high in the root tip, as shown in the Arabidopsis eFP Browser.[30] The NPC is disassembled simultaneously with nuclear membrane breakdown (NEBD) during mitotic entry, and Nups diffuse into the cytoplasm.[31] The outer ring of the NPC, including Nup85 and Nup133, is considered to maintain a subcomplex status during the mitotic phase,[32,33] and its localization varies among eukaryotes.[34] NUA localization also differs among eukaryotes,[35] but whether the nuclear basket of the NPC, including NUA, maintains a subcomplex status remains unclear. Super-resolution live imaging showed that Nup85-GFP and NUA-EYFP formed foci around kinetochores, visualized by tdTomato-CENH3, in metaphase (Figure 2A). The foci of NUA-EYFP were clearly colocalized with the CENH3 marker, while those of Nup85-GFP were closely localized near CENH3 but not colocalized. In addition, super-resolution live imaging of interphase nuclei of complementation lines showed that multiple signals of Nup colocalized with one CENH3 signal (Figures 2B and S3). Nup93b-EYFP also colocalized with the CENH3 signal (Figures 2B and S3). Our previous study suggested that the mechanism of centromere distribution in *A. thaliana* is composed of a two-step process: (i) scattering of centromeres by CII-LINC from anaphase to telophase, and (ii) stabilization of the positions of centromeres by CRWNs during interphase.[18] Because Nups required for centromere arrangement localized around centromeres in both metaphase and interphase, it is suggested that NPC is involved in two steps: (i) scattering centromeres and (ii) stabilizing their positions.

Nups regulate centromere scattering at the end of the mitotic phase

To investigate the relationship between the NPC and CII-LINC in centromere scattering, we performed time-lapse observation of centromeres in *nup85-2* and *nua-2* (Figure 3). As shown in our previous study, centromeres clustered at the spindle pole during late mitosis in

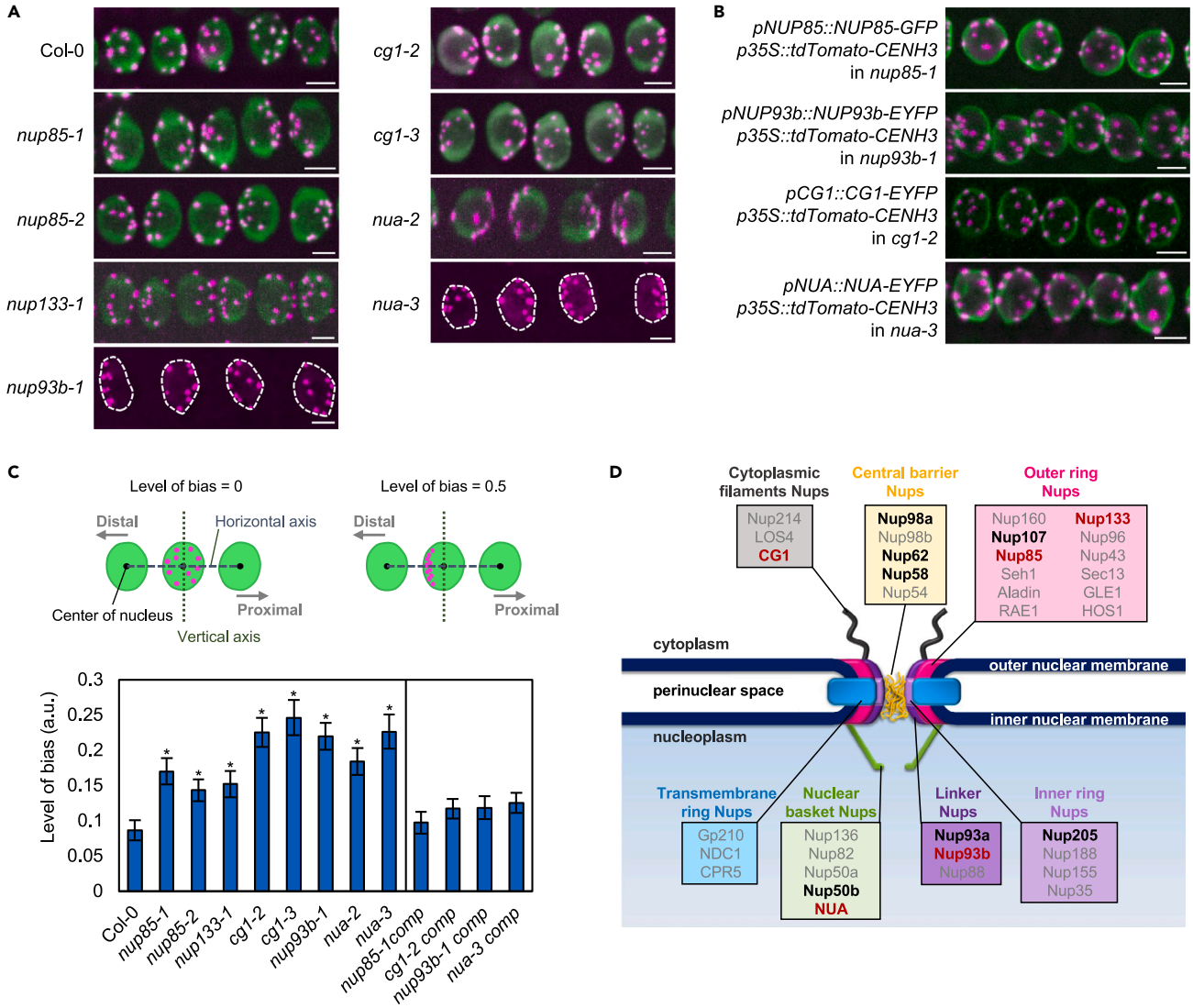

Figure 1. Function of Nups in centromere scattering

(A) Centromeres were visualized by *p35S::VENUS-CENH3* (magenta) in interphase nuclei in the meristematic zone (MZ) in *nup85-1*, *nup85-2*, *nup133-1*, *nup93b-1*, *cg1-2*, *cg1-3*, *nua-2*, and *nua-3*. Nuclei were visualized by *pRPS5a::H2B-tdTomato* (green). As for *nup93b-1* and *nua-3*, the outline of the nucleus is shown with a dashed line. Centromeres and nuclei were visualized by *p35S::tdTomato-CENH3* (magenta) and *pRPS5a::H2B-GFP* (green) in Col-0. The images are shown as standard deviation z-projections. Bars: 5 μm.

(B) Centromeres were visualized by *p35S::tdTomato-CENH3* (magenta) in interphase nuclei in the MZ in complementation lines. Nups were visualized by *pNUP85::NUP85-GFP*, *pNUP93b::NUP93b-EYFP*, *pCG1::CG1-EYFP*, and *pNUA::NUA-EYFP* in each of the complementation lines. Bars: 5 μm.

(C) The level of bias in centromere distribution in Col-0, *nup* mutants, and complementation lines was analyzed using the method presented in our previous paper.[18] In this analysis, the level of bias of the nucleus with scattered centromeres is close to 0, while that of the nucleus with biased centromeres is close to 0.5. The mean of the level of bias ±s.e.m. is shown in the graph. n > 20, *p < 0.05 by Student's t test. a.u., arbitrary units.

(D) Schematic diagram of the NPC in *A. thaliana*. Nups involved in centromere scattering are shown in red and other Nups whose mutant showed the normal centromere distribution (Figure S2) are shown in bold. See also Figure S1.

cap-h2-2 (Figure 3), indicating that CII-LINC functions in centromere scattering from anaphase to telophase.[18] The time-lapse observation revealed that, also in *nup85-2* and *nua-2*, centromeres remained at the spindle pole side after chromosome segregation in anaphase (2.5–7.5 min in Figure 3). This centromere distribution lasted during the subsequent G_1 phase (25–45 min in Figure 3). This indicates that Nup85 and NUA function simultaneously with condensin II, suggesting that the NPC and CII-LINC function cooperatively to regulate the scattering of centromeres. Meanwhile, focusing on the H2B fluorescent pattern, we found that, unlike in the wild type and *cap-h2-2*, chromatin decondensation did not occur at 10 min in *nup85-2* and *nua-2*, implying a delay in mitosis.

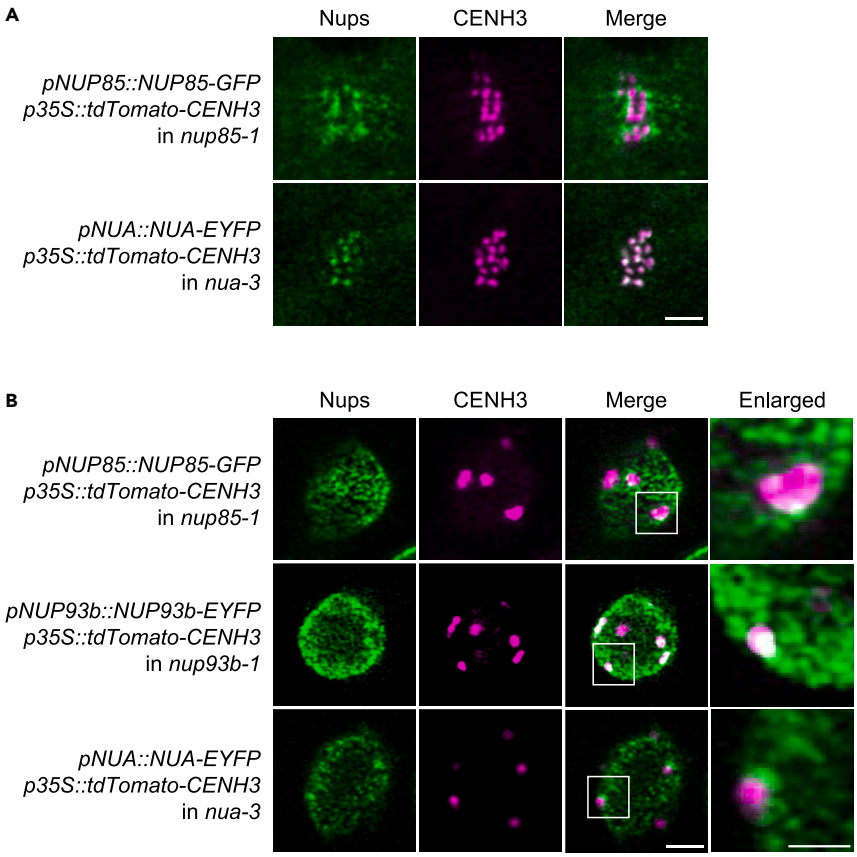

Figure 2. Nups localized to centromeres in metaphase and interphase

(A) Nups were visualized by *pNUP85::NUP85-GFP* or *pNUA::NUA-EYFP* (green), and centromeres were visualized by *p35S::tdTomato-CENH3* (magenta) in metaphase nuclei in the MZ. Bar: 2 μm. Of the multiple z axis images taken, the one z-plane closest to the center of the nucleus is shown.

(B) Nups were visualized by *pNUP85::NUP85-GFP*, *pNup93b::Nup93b-EYFP*, or *pNUA::NUA-EYFP* (green), and centromeres were visualized by *p35S::tdTomato-CENH3* (magenta) in interphase nuclei in the MZ. Bar for three leftmost rows: 2 μm, and bar for enlarged images: 1 μm. Of the multiple z axis images taken, one z-plane is shown. See also Figure S3.

The NPC is involved in centromere scattering, likely cooperating with the LINC complex

Next, we analyzed the physical interaction between the NPC and the LINC complex by co-immunoprecipitation (Co-IP). We used a transient protein expression system in *Nicotiana benthamiana* leaves. Because the molecular weight of NUA-EYFP is large (264 kDa) and it is expected to be difficult to detect, we focused on Nup85 and CG1, the smallest of the five Nups involved in centromere distribution. The interactions between Nup85 and SUN1 and between CG1 and SUN1 were verified by Co-IP (Figures 4A and S4), suggesting the potential association between these proteins in *A. thaliana*. We also investigated the genetic relationship between the NPC and the LINC complex by crossbreeding to further investigate whether these two factors function independently or cooperatively in centromere distribution. We focused on a mutant of the LINC complex, *sine1-1*, which shows a less biased centromere arrangement than the condensin II mutants[18] and generated the *nup85-2 sine1-1* double mutant introduced with *p35S::VENUS-CENH3*. The double mutant showed a biased centromere distribution (Figure 4B), and there was no statistically significant difference in the degree of bias between the double mutant and the respective single mutants (Figure 4C). Because the phenotype of the double mutant was not additive to that of each of the single mutants, it is suggested that the NPC functions in centromere scattering through the same pathway as the LINC complex, further supporting our hypothesis that the NPC and CII-LINC regulate centromere scattering cooperatively.

Nups do not function in stabilizing the position of centromeres

We next investigated whether the NPC is involved in stabilizing the positions of centromeres like CRWN1/4. Our previous study showed that the velocity of centromere movement in interphase nuclei was increased in *crwn1/4* double mutants.[18] Therefore, we performed time-lapse observations in each of the *nup* mutants, which showed a biased centromere distribution (Figure 1A), and analyzed the dynamics of centromeres. The results revealed that none of the *nup* mutants showed significant change in the dynamics of centromeres (Figure 5A). The velocity

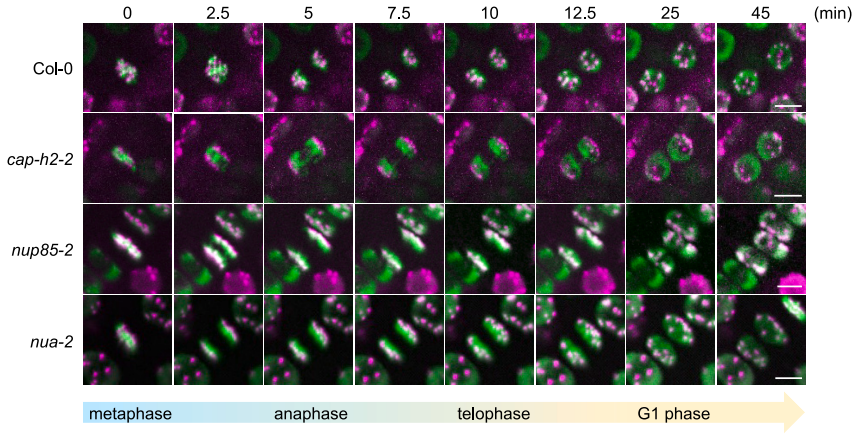

Figure 3. Nups regulate centromere scattering at the end of the mitotic phase

Time-lapse observations of centromeres (magenta) visualized by *p35S::tdTomato-CENH3* in Col-0 and *cap-h2-2* and by *p35S::VENUS-CENH3* in *nup85-2* and *nua-2*. Nuclei (green) were visualized by *pRPS5a::H2B-GFP* in Col-0 and *cap-h2-2* and by *pRPS5a::H2B-tdTomato* in *nup85-2* and *nua-2*. The images are shown as standard deviation z-projections. Bars: 5 μm.

of centromere movement was not increased like in *crwn1/4* double mutants (Figure 5B), suggesting that the NPC is not involved in stabilizing the positions of centromeres.

DISCUSSION

We revealed that the NPC functions in the arrangement of centromeres in *A. thaliana*. The NPC regulates centromere scattering, the first step of the two-step regulatory mechanism proposed in our previous study.[18] The NPC may function cooperatively with CII-LINC, forming the complex CII-LINC-NPC, and scatter centromeres from anaphase to telophase (Figure 6). The formation of this complex might be initiated in metaphase (Figure 6).

This study is the first to reveal the involvement of the NPC in the arrangement of centromeres among eukaryotes. Among organisms that adopt the non-Rabl orientation, humans and *A. thaliana* are the most well studied. In humans, a model was proposed that condensin II scatters centromeres via lengthwise compaction of chromosomes during or immediately after mitosis.[17] Meanwhile, in *A. thaliana*, we proposed a different model in that CII-LINC scatters centromeres.[18] Our results in this study provide further evidence supporting the idea that nuclear membrane proteins function in centromere scattering in plants. This mechanistic difference between animals and plants might be due to the subnuclear positioning of centromeres in interphase. In *A. thaliana*, centromeres localize to the nuclear periphery throughout the

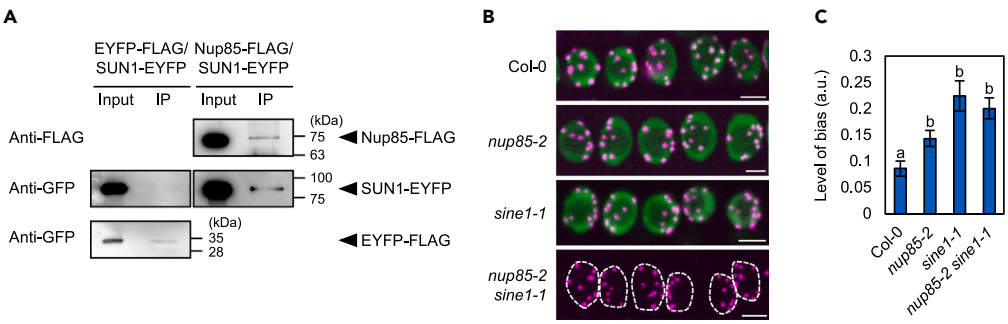

Figure 4. Nups underwent physical and genetic interaction with the LINC complex

(A) The interaction between SUN1 and Nup85 in *N. benthamiana* was detected by Co-IP with anti-GFP and anti-FLAG antibodies. *p35S::SUN1-EYFP* and *p35S::EYFP-FLAG* were infiltrated into *N. benthamiana* leaves for the control sample, and *p35S::SUN1-EYFP* and *p35S::Nup85-FLAG* were infiltrated for detection of the interaction. Proteins were extracted and immunoprecipitated with an anti-FLAG antibody. See also Figure S4.

(B) Centromeres (magenta) in interphase nuclei in the MZ were visualized by *p35S::tdTomato-CENH3* in Col-0 and *sine1-1* and by *p35S::VENUS-CENH3* in *nup85-2* and *nup85-2 sine1-1*. Nuclei (green) were visualized by *pRPS5a::H2B-GFP* in Col-0 and *sine1-1* and by *pRPS5a::H2B-tdTomato* in *nup85-2*. As for *nup85-2 sine1-1*, the outline of the nucleus is shown with a dashed line. The images are shown as standard deviation z-projections. Bars: 5 μm.

(C) The level of bias in centromere distribution in Col-0, *nup85-2*, *sine1-1*, and *nup85-2 sine1-1* measured from images in (B). The mean of the level of bias ± s.e.m. is shown in the graph. $n > 20$, $p < 0.05$ by Steel-Dwass test. Different letters indicate significantly different values. Data for *sine1-1* are from our previous paper.[18] a.u., arbitrary units.

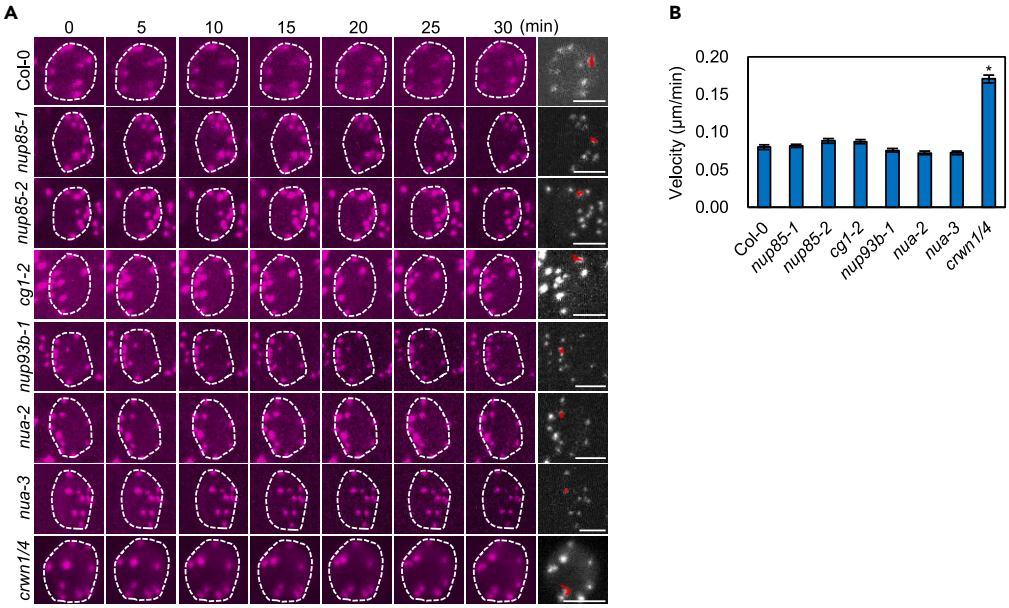

Figure 5. Nups do not function in stabilizing the position of centromeres

(A) Time-lapse observations of centromeres (magenta) visualized by *p35S::tdTomato-CENH3* in Col-0 and *crwn1/4*, and by *p35S::VENUS-CENH3* in *nup85-1*, *nup85-2*, *cg1-2*, *nup93b-1*, *nua-2*, and *nua-3* in interphase nuclei in the MZ (5 min intervals). The outline of the nucleus is shown with a dashed line. The images are shown as standard deviation z-projections. Red lines in the right panel show the trajectories of the centromere during observations at 30 min intervals in each line. Bars: 5 μm.

(B) The velocity of centromeres in interphase nuclei was calculated from images shown in (A). The mean of velocity ±s.e.m. is shown in the graph. n > 40, *p < 0.01 by Student's t test. Data for *crwn1/4* are from our previous paper.[18]

interphase.[36] However, in humans, centromeres are located in the nucleoplasm in the early G_1 phase and gradually move to the nuclear periphery in the late G_1 phase.[37,38] The involvement of the nuclear membrane proteins in centromere scattering may be limited to organisms whose centromeres are fixed to the nuclear periphery during interphase.

It is highly possible that the NPC functions in centromere scattering because mutants of Nups from different subcomplexes, Nup85, Nup133, CG1, NUA, and Nup93b, showed a biased centromere distribution. However, upon considering a previous study on budding yeast, another hypothesis arises. In budding yeast, several Nups together with the silencing factor Sir4, the inner nuclear membrane protein Esc1, and the SUMO E3 ligase Siz2 form a unique complex that differs from the canonical NPC and regulates heterochromatin organization and the nuclear periphery localization of the subtelomeric region.[39] We cannot rule out the possibility that Nup85, Nup133, CG1, NUA, and Nup93b form a unique complex that regulates centromere scattering.

We have identified that Nup85 and NUA localize around the kinetochore in metaphase. Nups diffuse into the cytoplasm during NEBD,[31] and their localization during mitosis varies among Nups and organisms.[34] On the basis of our results, the localization of plant Nup85 was similar to that of humans and *Caenorhabditis elegans*.[40–42] Meanwhile, the localization of NUA was not similar to that of any other eukaryotes. The NUA homolog in *D. melanogaster,* Megator, localizes near spindle microtubules.[43] In addition, the NUA homolog in humans, translocated promoter region (Tpr), diffuses into the cytoplasm in metaphase.[44,45] The unique localization of plant NUA may be related to the plant-specific regulation of centromere arrangement at the nuclear periphery.

We have proposed a model in which CII-LINC-NPC scatters centromeres from anaphase to telophase, and the formation of this complex starts in metaphase (Figure 6). Because condensin II localizes to centromeres throughout mitosis,[18] Nup85, NUA, and condensin II may interact in metaphase. In particular, we expect that condensin II and NUA interact because they have similar localization patterns to form foci and colocalize with centromeres in metaphase[18] (Figure 2). Meanwhile, a previous study reported that SUN1 diffuses around the spindle and does not localize to the kinetochore during metaphase.[46] From this, we expect that a CII-Nups complex is formed in metaphase, which becomes CII-LINC-NPC and regulates centromere scattering in anaphase. In eukaryotes, there are two NPC assembly pathways: postmitotic and interphase NPC assembly.[47] Around the centromere, NPC assembly occurs more slowly than in other chromatin regions because of the existence of spindle microtubules: NPC assembly is completed in G_1 phase.[47] In humans, Nups localize to the centromere region in the order of Nup153, Pom121, the outer ring, Tpr, Nup214, the central ring complex (the inner ring, the linker, and the channel), and Nup358.[45] Because the human Nup153 homolog Nup136 has been reported to diffuse into the cytoplasm in metaphase and there is no homolog of Pom121 in plants,[48] together with our observations (Figure 2A), we hypothesize that the outer ring and NUA (human Tpr homolog) are the first Nups that localize to the kinetochores in plants. However, other Nups that comprise the nuclear basket and the transmembrane ring may have similar functions to Nup153 and Pom121. Which Nups localize first to centromeres during mitosis needs further investigation in future work. We

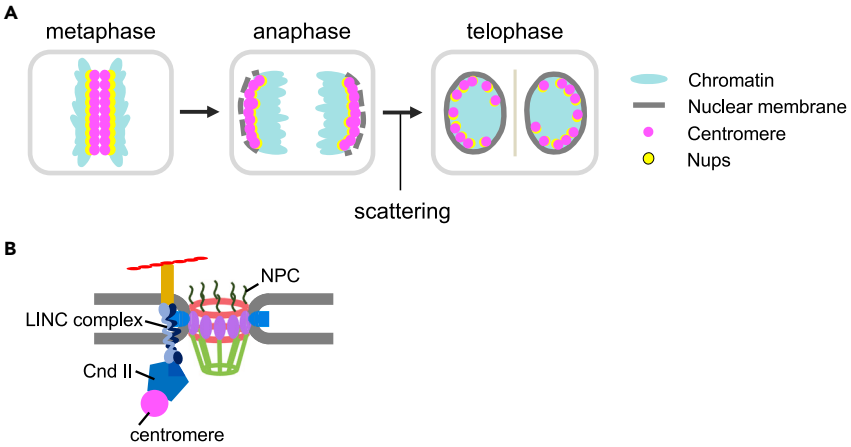

Figure 6. Schematic model of centromere scattering by CII-LINC and the NPC

(A) In metaphase, Nup85 and NUA localize to centromeres. From anaphase to telophase, CII-LINC and the NPC form the CII-LINC-NPC complex shown in (B) and regulate centromere scattering.

(B) Schematic diagram of CII-LINC-NPC complex.

predict that the CII-NPC is completed when other Nups gather around Nup85 and NUA in CII-Nups as landmarks. The interactions between SUN1 and Nup85 (Figure 4A) and between SUN1 and CG1 (Figure S4) suggested the interaction between the LINC complex and the NPC. However, the actual process by which CII-LINC-NPCs are formed needs to be analyzed in more detail in future work.

Our study revealed that the NPC is involved in the two-step regulation of centromere arrangement. Although we have elucidated several factors regulating centromere scattering, how these factors spread centromeres remains unclear. Future work should clarify this mechanism and provide insight into the biological significance of proper centromere distribution in interphase nuclei.

Limitations of the study

Although we investigated mutants of 12 out of 35 Nups in *A. thaliana*, we cannot rule out the possibility that some of the 23 Nups not examined in this study are also involved in centromere distribution. Future studies using other *nup* mutants should provide insight into the features of Nups involved in centromere arrangement. Moreover, it remains unclear whether all NPCs on the nuclear membrane (at least several hundred) form a giant complex with CII-LINC and regulate centromere positioning because the number of NPCs colocalized with centromeres was a small fraction of the total (Figure 2B). It is possible that only some NPCs are involved in regulating centromere arrangement or that the five Nups identified in this study form a unique complex distinct from NPCs to regulate centromere arrangement. Simultaneous visualization of Nups involved in centromere scattering and Nups not involved in it (e.g., Nup98a, Nup62, and Nup58) should provide insight by observing their colocalization at the nuclear membrane.

STAR★METHODS

Detailed methods are provided in the online version of this paper and include the following:

- KEY RESOURCES TABLE
- RESOURCE AVAILABILITY
  - Lead contact
  - Materials availability
  - Data and code availability
- EXPERIMENTAL MODEL AND STUDY PARTICIPANT DETAILS
  - A. thaliana
  - N. benthamiana
  - Bacterial strains
- METHOD DETAILS
  - qRT-PCR
  - Generation of transgenic plants
  - Confocal imaging
  - Co-IP assays
- QUANTIFICATION AND STATISTICAL ANALYSIS

SUPPLEMENTAL INFORMATION

Supplemental information can be found online at https://doi.org/10.1016/j.isci.2024.108855.

ACKNOWLEDGMENTS

We thank T. Sugiyama and Y. Asako (Tokyo University of Science, Chiba, Japan), and Y. Inui and S. Mibu (The University of Tokyo, Chiba, Japan) for substantial technical assistance, and Edanz (https://jp.edanz.com/ac) for editing a draft of this manuscript. The seed of *nup85-1* was kindly donated by Dr. Kentaro Tamura (University of Shizuoka, Shizuoka, Japan). This work was supported by grants from MXT/JSPS KAKENHI (20H03297 and 22H00415), JST CREST (JPMJCR20S6) to S.M., and grants from Takeda Science Foundation and MXT/JSPS KAKENHI (23H02511) to T.S.

AUTHOR CONTRIBUTIONS

T.S., Y.S., H.S., and S.M. designed the experiments. N.I., Y.O., S.H., Y.S., and T.S. conducted the experiments and analyzed data. N.I., T.S., H.S., and S.M. wrote the manuscript. All authors contributed through discussions and reviewed the manuscript.

DECLARATION OF INTERESTS

The authors declare no competing interests.

Received: May 6, 2023
Revised: November 28, 2023
Accepted: January 5, 2024
Published: January 11, 2024

REFERENCES

1. Cleveland, D.W., Mao, Y., and Sullivan, K.F. (2003). Centromeres and kinetochores: from epigenetics to mitotic checkpoint signaling. Cell *112*, 407–421.
2. Rabl, C. (1885). Über zellthilung. Morphol Jahrb *10*, 214–330.
3. Dong, F., and Jiang, J. (1998). Non-Rabl patterns of centromere and telomere distribution in the interphase nuclei of plant cells. Chromosome Res. *6*, 551–558.
4. Schubert, I., and Shaw, P. (2011). Organization and dynamics of plant interphase chromosomes. Trends Plant Sci. *16*, 273–281.
5. Santos, A.P., and Shaw, P. (2004). Interphase chromosomes and the Rabl configuration: does genome size matter? J. Microsc. *214*, 201–206.
6. Oko, Y., Ito, N., and Sakamoto, T. (2020). The mechanisms and significance of the positional control of centromeres and telomeres in plants. J. Plant Res. *133*, 471–478.
7. Funabiki, H., Hagan, I., Uzawa, S., and Yanagida, M. (1993). Cell cycle-dependent specific positioning and clustering of centromeres and telomeres in fission yeast. J. Cell Biol. *121*, 961–976.
8. Jin, Q., Trelles-Sticken, E., Scherthan, H., and Loidl, J. (1998). Yeast nuclei display prominent centromere clustering that is reduced in nondividing cells and in meiotic prophase. J. Cell Biol. *141*, 21–29.
9. Hochstrasser, M., Mathog, D., Gruenbaum, Y., Saumweber, H., and Sedat, J.W. (1986). Spatial organization of chromosomes in the salivary gland nuclei of Drosophila melanogaster. J. Cell Biol. *102*, 112–123.
10. Billia, F., and de Boni, U. (1991). Localization of centromeric satellite and telomeric DNA sequences in dorsal root ganglion neurons, *in vitro*. J. Cell Sci. *100*, 219–226.
11. Fransz, P., De Jong, J.H., Lysak, M., Castiglione, M.R., and Schubert, I. (2002). Interphase chromosomes in *Arabidopsis* are organized as well defined chromocenters from which euchromatin loops emanate. Proc. Natl. Acad. Sci. USA *99*, 14584–14589.
12. Weierich, C., Brero, A., Stein, S., von Hase, J., Cremer, C., Cremer, T., and Solovei, I. (2003). Three-dimensional arrangements of centromeres and telomeres in nuclei of human and murine lymphocytes. Chromosome Res *11*, 485–502. https://doi.org/10.1023/a:1025016828544.
13. Lilly, M.A., and Duronio, R.J. (2005). New insights into cell cycle control from the *Drosophila* endocycle. Oncogene *24*, 2765–2775.
14. Dej, K.J., and Spradling, A.C. (1999). The endocycle controls nurse cell polytene chromosome structure during *Drosophila* oogenesis. Development *126*, 293–303.
15. Bauer, C.R., Hartl, T.A., and Bosco, G. (2012). Condensin II promotes the formation of chromosome territories by inducing axial compaction of polyploid interphase chromosomes. PLoS Genet. *8*, e1002873.
16. Hirano, T. (2005). Condensins: organizing and segregating the genome. Curr Biol *15*, R265–R275. https://doi.org/10.1016/j.cub.2005.03.037.
17. Hoencamp, C., Dudchenko, O., Elbatsh, A.M.O., Brahmachari, S., Raaijmakers, J.A., van Schaik, T., Sedeño Cacciatore, Á., Contessoto, V.G., van Heesbeen, R.G.H.P., van den Broek, B., et al. (2021). 3D genomics across the tree of life reveals condensin II as a determinant of architecture type. Science *372*, 984–989.
18. Sakamoto, T., Sakamoto, Y., Grob, S., Slane, D., Yamashita, T., Ito, N., Oko, Y., Sugiyama, T., Higaki, T., Hasezawa, S., et al. (2022). Two-step regulation of centromere distribution by condensin II and the nuclear envelope proteins. Nat. Plants *8*, 940–953.
19. Meier, I., Richards, E.J., and Evans, D.E. (2017). Cell Biology of the Plant Nucleus. Annu. Rev. Plant Biol. *68*, 139–172.
20. Sakamoto, Y., Sato, M., Sato, Y., Harada, A., Suzuki, T., Goto, C., Tamura, K., Toyooka, K., Kimura, H., Ohkawa, Y., et al. (2020). Subnuclear gene positioning through lamina association affects copper tolerance. Nat. Commun. *11*, 5914.
21. Ito, N., Sakamoto, T., and Matsunaga, S. (2021). Components of the Nuclear Pore Complex are Rising Stars in the Formation of a Subnuclear Platform of Chromatin Organization beyond Their Structural Role as a Nuclear Gate. Cytologia *86*, 183–187.
22. Alber, F., Dokudovskaya, S., Veenhoff, L.M., Zhang, W., Kipper, J., Devos, D., Suprapto, A., Karni-Schmidt, O., Williams, R., Chait, B.T., et al. (2007). The molecular architecture of the nuclear pore complex. Nature *450*, 695–701.
23. Tamura, K., and Hara-Nishimura, I. (2013). The molecular architecture of the plant nuclear pore complex. J. Exp. Bot. *64*, 823–832.
24. Cronshaw, J.M., Krutchinsky, A.N., Zhang, W., Chait, B.T., and Matunis, M.J. (2002). Proteomic analysis of the mammalian nuclear pore complex. J. Cell Biol. *158*, 915–927.
25. Rout, M.P., Aitchison, J.D., Suprapto, A., Hjertaas, K., Zhao, Y., and Chait, B.T. (2000). The yeast nuclear pore complex: composition, architecture, and transport mechanism. J. Cell Biol. *148*, 635–651.
26. Knockenhauer, K.E., and Schwartz, T.U. (2016). The Nuclear Pore Complex as a Flexible and Dynamic Gate. Cell *164*, 1162–1171.
27. Kuhn, T.M., and Capelson, M. (2019). Nuclear Pore Proteins in Regulation of Chromatin State. Cells *8*.
28. Lamm, N., Rogers, S., and Cesare, A.J. (2021). Chromatin mobility and relocation in DNA repair. Trends Cell Biol. *31*, 843–855.
29. Bi, X., Cheng, Y.J., Hu, B., Ma, X., Wu, R., Wang, J.W., and Liu, C. (2017). Nonrandom

domain organization of the *Arabidopsis* genome at the nuclear periphery. Genome Res. *27*, 1162–1173.

30. Winter, D., Vinegar, B., Nahal, H., Ammar, R., Wilson, G.V., and Provart, N.J. (2007). An "Electronic Fluorescent Pictograph" browser for exploring and analyzing large-scale biological data sets. PLoS One *2*, e718.
31. Dultz, E., Zanin, E., Wurzenberger, C., Braun, M., Rabut, G., Sironi, L., and Ellenberg, J. (2008). Systematic kinetic analysis of mitotic dis- and reassembly of the nuclear pore in living cells. J. Cell Biol. *180*, 857–865.
32. Heusel, M., Frank, M., Köhler, M., Amon, S., Frommelt, F., Rosenberger, G., Bludau, I., Aulakh, S., Linder, M.I., Liu, Y., et al. (2020). A Global Screen for Assembly State Changes of the Mitotic Proteome by SEC-SWATH-MS. Cell Syst. *10*, 133–155.e6.
33. Orjalo, A.V., Arnaoutov, A., Shen, Z., Boyarchuk, Y., Zeitlin, S.G., Fontoura, B., Briggs, S., Dasso, M., and Forbes, D.J. (2006). The Nup107-160 nucleoporin complex is required for correct bipolar spindle assembly. Mol. Biol. Cell *17*, 3806–3818.
34. Chatel, G., and Fahrenkrog, B. (2011). Nucleoporins: leaving the nuclear pore complex for a successful mitosis. Cell. Signal. *23*, 1555–1562.
35. Mossaid, I., and Fahrenkrog, B. (2015). Complex Commingling: Nucleoporins and the Spindle Assembly Checkpoint. Cells *4*, 706–725.
36. Fang, Y., and Spector, D.L. (2005). Centromere positioning and dynamics in living *Arabidopsis* plants. Mol. Biol. Cell *16*, 5710–5718.
37. Solovei, I., Schermelleh, L., Düring, K., Engelhardt, A., Stein, S., Cremer, C., and Cremer, T. (2004). Differences in centromere positioning of cycling and postmitotic human cell types. Chromosoma *112*, 410–423.
38. van Schaik, T., Vos, M., Peric-Hupkes, D., Hn Celie, P., and van Steensel, B. (2020). Cell cycle dynamics of lamina-associated DNA. EMBO Rep. *21*, e50636.
39. Lapetina, D.L., Ptak, C., Roesner, U.K., and Wozniak, R.W. (2017). Yeast silencing factor Sir4 and a subset of nucleoporins form a complex distinct from nuclear pore complexes. J. Cell Biol. *216*, 3145–3159.
40. Loïodice, I., Alves, A., Rabut, G., Van Overbeek, M., Ellenberg, J., Sibarita, J.B., and Doye, V. (2004). The entire Nup107-160 complex, including three new members, is targeted as one entity to kinetochores in mitosis. Mol. Biol. Cell *15*, 3333–3344.
41. Belgareh, N., Rabut, G., Baï, S.W., van Overbeek, M., Beaudouin, J., Daigle, N., Zatsepina, O.V., Pasteau, F., Labas, V., Fromont-Racine, M., et al. (2001). An evolutionarily conserved NPC subcomplex, which redistributes in part to kinetochores in mammalian cells. J. Cell Biol. *154*, 1147–1160.
42. Franz, C., Walczak, R., Yavuz, S., Santarella, R., Gentzel, M., Askjaer, P., Galy, V., Hetzer, M., Mattaj, I.W., and Antonin, W. (2007). MEL-28/ELYS is required for the recruitment of nucleoporins to chromatin and postmitotic nuclear pore complex assembly. EMBO Rep. *8*, 165–172.
43. Lince-Faria, M., Maffini, S., Orr, B., Ding, Y., Florindo, C., Sunkel, C.E., Tavares, Á., Johansen, J., Johansen, K.M., and Maiato, H. (2009). Spatiotemporal control of mitosis by the conserved spindle matrix protein Megator. J. Cell Biol. *184*, 647–657.
44. Rodriguez-Bravo, V., Maciejowski, J., Corona, J., Buch, H.K., Collin, P., Kanemaki, M.T., Shah, J.V., and Jallepalli, P.V. (2014). Nuclear pores protect genome integrity by assembling a premitotic and Mad1-dependent anaphase inhibitor. Cell *156*, 1017–1031.
45. Otsuka, S., Tempkin, J.O.B., Zhang, W., Politi, A.Z., Rybina, A., Hossain, M.J., Kueblbeck, M., Callegari, A., Koch, B., Morero, N.R., et al. (2023). A quantitative map of nuclear pore assembly reveals two distinct mechanisms. Nature *613*, 575–581.
46. Oda, Y., and Fukuda, H. (2011). Dynamics of Arabidopsis SUN proteins during mitosis and their involvement in nuclear shaping. Plant J. *66*, 629–641.
47. Kutay, U., Jühlen, R., and Antonin, W. (2021). Mitotic disassembly and reassembly of nuclear pore complexes. Trends Cell Biol. *31*, 1019–1033.
48. Tamura, K., Fukao, Y., Iwamoto, M., Haraguchi, T., and Hara-Nishimura, I. (2010). Identification and characterization of nuclear pore complex components in *Arabidopsis thaliana*. Plant Cell *22*, 4084–4097.
49. Adachi, S., Minamisawa, K., Okushima, Y., Inagaki, S., Yoshiyama, K., Kondou, Y., Kaminuma, E., Kawashima, M., Toyoda, T., Matsui, M., et al. (2011). Programmed induction of endoreduplication by DNA double-strand breaks in *Arabidopsis*. Proc. Natl. Acad. Sci. USA *108*, 10004–10009.
50. Zhou, X., Graumann, K., Wirthmueller, L., Jones, J.D.G., and Meier, I. (2014). Identification of unique SUN-interacting nuclear envelope proteins with diverse functions in plants. J. Cell Biol. *205*, 677–692.
51. Sakamoto, T., Inui, Y.T., Uraguchi, S., Yoshizumi, T., Matsunaga, S., Mastui, M., Umeda, M., Fukui, K., and Fujiwara, T. (2011). Condensin II alleviates DNA damage and is essential for tolerance of boron overload stress in *Arabidopsis*. Plant Cell *23*, 3533–3546.
52. Curtis, M.D., and Grossniklaus, U. (2003). A gateway cloning vector set for high-throughput functional analysis of genes in planta. Plant Physiol. *133*, 462–469.
53. Clough, S.J., and Bent, A.F. (1998). Floral dip: a simplified method for *Agrobacterium*-mediated transformation of *Arabidopsis thaliana*. Plant J. *16*, 735–743.
54. Sato, H., Mizoi, J., Tanaka, H., Maruyama, K., Qin, F., Osakabe, Y., Morimoto, K., Ohori, T., Kusakabe, K., Nagata, M., et al. (2014). *Arabidopsis* DPB3-1, a DREB2A interactor, specifically enhances heat stress-induced gene expression by forming a heat stress-specific transcriptional complex with NF-Y subunits. Plant Cell *26*, 4954–4973. https://doi.org/10.1105/tpc.114.132928.

STAR★METHODS

KEY RESOURCES TABLE

REAGENT or RESOURCE	SOURCE	IDENTIFIER
Antibodies		
Anti-GFP antibody	Abcam	Cat#ab290; RRID: AB_303395
Anti-FLAG antibody	Wako	Cat#018-22381; RRID: AB_10659453
Monoclonal ANTI-FLAG® M2 antibody	Sigma-Aldrich	Cat#F3165; RRID: AB_259529
Anti-IgG (H+L chain) (Rabbit) pAb-HRP	MBL	Cat#458; RRID: AB_2827722
Anti-Mouse IgG (H+L) Antibody, HRP Conjugated	Promega	Cat#W402B; RRID: AB_430834
Bacterial and virus strains		
Agrobacterium tumefaciens GV3101	Sakamoto et al., 2022[18]	N/A
Escherichia coli DH5α	Sakamoto et al., 2022[18]	N/A
Chemicals, peptides, and recombinant proteins		
MG132	Wako	Cat#139-18451
cOmplete™, EDTA-free Protease Inhibitor Cocktail	Sigma-Aldrich	Cat#5056489001
Critical commercial assays		
Maxwell® RSC Plant RNA Kit	Promega	Cat#AS1500
Verso cDNA Synthesis Kit	Thermo Scientific	Cat#AB1453B
Luna Universal qPCR Master Mix	New England Biolabs	Cat#M3003
pENTR™/D-TOPO™ Cloning Kit	Invitrogen	Cat#K240020SP
Gateway™ LR Clonase™ II Enzyme mix	Invitrogen	Cat#11791020
μMACS GFP Isolation Kit	Miltenyi Biotec	Cat#130-091-125
Anti-DYKDDDDK antibody-conjugated magnetic beads	Wako	Cat#011-25154
ImmunoStar LD	Wako	Cat#296-69901
Deposited data		
The level of bias in centromere distribution in *sine1-1*	Sakamoto et al., 2022[18]	N/A
The velocity of centromeres in *crwn1/4*	Sakamoto et al., 2022[18]	N/A
Co-IP of the interaction between SUN1-Nup85 and SUN1-CG1	This paper, Mendeley	Figures 4 and S4; https://doi.org/10.17632/yp9sxcn4b4.1
Experimental models: organisms/strains		
Arabidopsis: Col-0	Sakamoto et al., 2022[18]	N/A
Arabidopsis: *cg1-2*	ABRC	SALK_063511
Arabidopsis: *cg1-3*	ABRC	SALK_006526C
Arabidopsis: *nup98a-1*	ABRC	SALK_103803C
Arabidopsis: *nup62-5*	ABRC	SALK_208991C
Arabidopsis: *nup58-5*	ABRC	SAIL_349_B01
Arabidopsis: *nup50b-1*	ABRC	SAIL_1284_E09
Arabidopsis: *nua-2*	ABRC	SALK_069922C
Arabidopsis: *nua-3*	ABRC	SAIL_505_H11
Arabidopsis: *nup93a-1*	ABRC	SALK_137170C
Arabidopsis: *nup93b-1*	ABRC	SAIL_94_A05
Arabidopsis: *nup205-2*	ABRC	SAIL_874_A02
Arabidopsis: *nup133-1*	ABRC	SALK_092608C

(*Continued on next page*)

Continued

REAGENT or RESOURCE	SOURCE	IDENTIFIER
Arabidopsis: *nup133-4*	ABRC	SALK_029895C
Arabidopsis: *nup107-1*	ABRC	SALK_057072C
Arabidopsis: *nup85-1*	A Gift from Dr. K. Tamura	SALK_133369C
Arabidopsis: *nup85-2*	ABRC	SALK_113274
Arabidopsis: *35S::tdTomato-CENH3/RPS5a::H2B-GFP*/Col-0, *cap-h2-2*, *sine1-1*, and *crwn1/4*	Sakamoto et al., 2022[18]	Transgenic Col-0, *cap-h2-2*, *sine1-1*, and *crwn1/4*
Arabidopsis: *35S::VENUS-CENH3/RPS5a::H2B-tdTomato/nup* mutant	This study	Transgenic *nup* mutants
Arabidopsis: *35S::VENUS-CENH3/nup85-2*	This study	Transgenic *nup85-2*
Arabidopsis: *sine1-1*	ABRC	SALK_018239C
Arabidopsis: *35S::VENUS-CENH3/nup85-2 sine1-1*	This study	Cross between *35S::VENUS-CENH3/nup85-2* and *sine1-1*
Arabidopsis: *NUP85::NUP85-GFP/35S::tdTomato-CENH3/nup85-1*	This study	Transgenic *nup85-1*
Arabidopsis: *NUP93b::NUP93b-EYFP/35S::tdTomato-CENH3/nup93b-1*	This study	Transgenic *nup93b-1*
Arabidopsis: *CG1::CG1-EYFP/35S::tdTomato-CENH3/cg1-2*	This study	Transgenic *cg1-2*
Arabidopsis: *NUA::NUA-EYFP/35S::tdTomato-CENH3/nua-3*	This study	Transgenic *nua-3*
Tobacco: *Nicotiana benthamiana*	Sakamoto et al., 2022[18]	N/A
Oligonucleotides		
Primers used are shown in Table S2	This study	N/A
Recombinant DNA		
p35S::tdTomato-CENH3	Sakamoto et al., 2022[18]	N/A
p35S::VENUS-CENH3	Sakamoto et al., 2022[18]	N/A
pRPS5a::H2B-tdTomato	Adachi et al., 2011[49]	N/A
pNUP85::NUP85-GFP	This study	N/A
pNUP93b::NUP93b-EYFP	This study	N/A
pCG1::CG1-EYFP	This study	N/A
pNUA::NUA-EYFP	This study	N/A
p35S::Nup85-FLAG	This study	N/A
p35S::SUN1-EYFP	This study	N/A
p35S::CG1-EYFP	This study	N/A
p35S::SUN1-FLAG	This study	N/A
p35S::EYFP-FLAG	This study	N/A
Software and algorithms		
ImageJ	NIH	https://imagej.nih.gov/ij/download.html
ZEN (blue edition v3.1)	ZEISS	N/A

RESOURCE AVAILABILITY

Lead contact

Further information and requests for resources and reagents should be directed to and will be fulfilled by the lead contact, Sachihiro Matsunaga (sachi@edu.k.u-tokyo.ac.jp).

Materials availability

This study did not generate new unique reagents.

Data and code availability

- Original western blot images have been deposited at Mendeley and are publicly available as of the date of publication. The DOI is listed in the key resources table.
- All data reported in this paper will be shared by the lead contact upon request.
- This paper does not report original code.
- Any additional information required to reanalyze the data reported in this paper is available from the lead contact upon request.

EXPERIMENTAL MODEL AND STUDY PARTICIPANT DETAILS

A. thaliana

The Columbia (Col-0) accession of *A. thaliana* was used in this study. The *sine1-1* (SALK_018239C) line was isolated in the previous study,[50] and *nup85-1* was donated by the University of Shizuoka, Shizuoka, Japan. Other *nup* mutants used in this study are listed in Table S1. Primers used for genotyping are listed in Table S2. In all experiments, seeds were sown on media containing MGRL solution,[51] 1% (w/v) sucrose, and 1.5% (w/v) gellan gum. After 1 day of incubation at 4°C, the plates were placed vertically in a growth chamber (16:8 h light/dark cycle, 22°C) until analysis.

N. benthamiana

Seeds of *N. benthamiana* were sown on soil mixed with vermiculite (Asahi Industry Co., Ltd.) and Jiffy mix (Sakata), and placed in a growth chamber (16 h light, 22°C/8 h dark, 20°C) until analysis.

Bacterial strains

Agrobacterium tumefaciens GV3101 was cultured at 28°C in LB medium containing appropriate antibiotics. *Escherichia coli* DH5α competent cells were cultured at 37°C in LB medium containing appropriate antibiotics.

METHOD DETAILS

qRT-PCR

One-week-old plants were used for qRT-PCR. RNA was extracted using a Maxwell® RSC Plant RNA Kit (Promega) and Maxwell® RSC Instrument (Promega), and reverse-transcribed using a Verso cDNA Synthesis Kit (Thermo Scientific). Gene expression was quantified using Luna Universal qPCR Master Mix (New England Biolabs) on Thermal Cycler Dice® Real Time System III (TaKaRa). *ACT2* was used as the internal control gene. Primers used in qRT-PCR are shown in Table S2.

Generation of transgenic plants

Col-0, *cap-h2-2* (SALK_059304), *sine1-1*, and *crwn1/4* (SALK_016800, SALK_079288) expressing *p35S::tdTomato-CENH3* and *pRPS5a::H2B-GFP* had been established previously.[18] To visualize centromeres, a pMDC99[52] vector containing *p35S::tdTomato-CENH3* and a pMDC99 vector containing *p35S::VENUS-CENH3* from our previous study were used.[18] To visualize nuclei, a pMDC99 vector containing *pRPS5a::H2B-tdTomato*[49] was used. To visualize Nups, an amplified clone of the genomic *NUP85*, *NUP93b*, *CG1*, and *NUA* fragments was subcloned into the pENTR-D/TOPO vector (Invitrogen), following the manufacturer's protocol. The genomic fragment of Nups was transferred to pGWB504 or pGWB540 harboring GFP or EYFP, respectively, by LR recombination with LR clonase II (Invitrogen), following the manufacturer's protocol, to construct a vector containing *pNUP85::NUP85-GFP*, *pNUP93b::NUP93b-EYFP*, *pCG1::CG1-EYFP*, and *pNUA::NUA-EYFP*. Primers used for cloning are listed in Table S2. The plasmid was transformed into *A. tumefaciens* (strain GV3101 pMP90) and transformed into plants by floral dip.[53] Transgenic plants were selected on medium containing 1/2× Murashige and Skoog salts, 1% sucrose, 20 μg ml^{-1} hygromycin B, and 100 μg ml^{-1} cefotaxime. The fluorescence of tdTomato, GFP, EYFP, and VENUS was confirmed in T1 plants. T1, T2, or T3 plants were used for the analysis. The *nup85-2 sine1-1* double mutant was generated by crossing *nup85-2* expressing *p35S::VENUS-CENH3* and *sine1-1*.

Confocal imaging

Five- to seven-day-old plants were used for confocal imaging. For super-resolution live imaging of NUP85-GFP, NUA-EYFP, and NUP93b-EYFP, the roots were observed under an LSM900 inverted laser confocal microscope equipped with Airyscan 2 (ZEISS), and images were processed by ZEN operating software (blue edition v3.1; ZEISS). To image NUP85-GFP, NUP93b-EYFP, CG1-EYFP, NUA-EYFP, tdTomato-CENH3, VENUS-CENH3, H2B-tdTomato, and H2B-GFP, the roots of the samples were observed under an inverted fluorescence microscope (IX81; Olympus), which included a laser (488 nm for GFP, EYFP, and VENUS, and 561 nm for tdTomato detection) equipped with a confocal scanning unit (CSU-X1; Yokogawa) and an Andor Neo 5.5 sCMOS camera (Oxford Instruments). The *z*-stacks were reconstructed into a standard deviation projection view using ImageJ software (https://imagej.nih.gov/ij/download.html). The trajectories of centromeres were analyzed using the ImageJ software plugin MTrackJ (https://imagescience.org/meijering/software/mtrackj/). The orthogonal view of the XZ plane and the intensity plot were produced using ImageJ software. All imaging analyses were repeated independently at least twice with similar results.

Co-IP assays

The coding sequences of *Nup85* and *CG1* without the stop codon were amplified from *A. thaliana* cDNA and the coding sequence of *EYFP* without the stop codon from pGWB541 vector. The clones of *Nup85*, *CG1*, and *EYFP* were subcloned into the pENTR-D/TOPO vector. As for *SUN1*, the entry clone we established previously[18] was used. By LR recombination with LR clonase II, the fragments of *CG1* and *SUN1* were transferred into the pGWB541 vector to construct Gateway destination vectors harboring *p35S::CG1-EYFP* and *p35S::SUN1-EYFP*. The fragment of *Nup85* and *SUN1* was transferred into the pGWB611 vector to construct *p35S::Nup85-FLAG* and *p35S::SUN1-FLAG*. The fragment of EYFP was transferred into pGWB511 to construct *p35S::EYFP-FLAG*. The plasmids were transformed into *A. tumefaciens* (strain GV3101 pMP90). Primers used for vector construction are listed in Table S2.

The fluorescent fusion proteins were transiently expressed in *N. benthamiana* leaves by *Agrobacterium*-mediated infiltration method.[54] Leaves were harvested 4 or 5 days after inoculation. Immunoprecipitation was performed using a μMACS GFP Isolation Kit (Miltenyi Biotec). Approximately 1.0 g of leaves were homogenized and dissolved in a solution containing 1978 μL of μMACS lysis buffer (Miltenyi Biotec), 2 μL of 10 mM MG132 (Wako), and 20 μL of 100× cOmplete™ (Sigma-Aldrich). In the experiment to investigate the interaction between Nup85-FLAG and SUN1-EYFP, the lysate was then filtered through two layers of Miracloth (Merck), mixed with anti-DYKDDDDK antibody-conjugated magnetic beads (Wako), and incubated at 4°C for 3 h. The FLAG-fusion proteins were purified using a magnetic column in accordance with the manufacturer's protocol. Anti-GFP antibody (ab290; Abcam) (1:2,000) and anti-FLAG antibody (clone 1E6; Wako) (1:10,000) were used as primary antibodies. Anti-IgG (H+L chain) (Rabbit) pAb-Horseradish peroxidase (HRP) (458, MBL) (1:10,000) and anti-mouse IgG (H+L) Antibody, HRP conjugate (W402B; Promega) (1:20,000), were used as secondary antibodies. In the experiment to investigate the interaction between CG1-EYFP and SUN1-FLAG, slight changes were made to the protocol as a result of examining the experimental conditions. The lysate was filtered through Cell Strainer (VCS-40; AS ONE Corporation), mixed with μMACS Anti-GFP MicroBeads from the μMACS GFP Isolation Kit (Miltenyi Biotec), and incubated at 4°C for 1 h. Anti-GFP antibody (ab290; Abcam) (1:2,000) and monoclonal Anti-FLAG® M2 antibody (F3165; Sigma-Aldrich) (1:1,000) were used as primary antibodies. Anti-IgG (H+L chain) (Rabbit) pAb-HRP (458, MBL) (1:5,000) and anti-mouse IgG (H+L) Antibody, HRP conjugate (W402B; Promega) (1:2,000), were used as the secondary antibodies. Chemiluminescence from the target proteins of each antibody was visualized using ImmunoStar LD (Wako) on a Fusion Pulse system (Vilber Lourmat). This experiment was independently repeated twice with similar results.

QUANTIFICATION AND STATISTICAL ANALYSIS

All quantitative data are shown as mean ± s.e.m. The value of n represents the number of analyzed nuclei or individual experiments. Details are provided in each figure legend. For the results presented in Figures 1C, 5B, S1, and S2B, Student's t-test was used for statistical analysis, with significant differences at $p < 0.05$ or $p < 0.01$ being marked with an asterisk. For the results in Figure 4C, Steel-Dwass test was used for statistical analysis, with a significant difference at $p < 0.05$ being marked with an asterisk.